Dendritic, Transferable, Strictly Monolayer MoS_2 Flakes Synthesized on $SrTiO_3$ Single Crystals for Efficient Electrocatalytic Applications

Yu Zhang,[†,‡] Qingqing Ji,[‡] Gao-Feng Han,[§] Jing Ju,[⊥] Jianping Shi,[†,‡] Donglin Ma,[‡] Jingyu Sun,[‡] Yanshuo Zhang,[†,‡] Minjie Li,[‡] Xing-You Lang,[§] Yanfeng Zhang,[†,‡,*] and Zhongfan Liu[‡]

[†]Department of Materials Science and Engineering, College of Engineering, Peking University, Beijing 100871, People's Republic of China, [‡]Center for Nanochemistry (CNC), Beijing National Laboratory for Molecular Sciences, College of Chemistry and Molecular Engineering, Peking University, Beijing 100871, People's Republic of China, [§]Key Laboratory of Automobile Materials (Jilin University), Ministry of Education, and School of Materials Science and Engineering, Jilin University, Changchun 130022, People's Republic of China, and [⊥]State Key Laboratory of Rare Earth Materials Chemistry and Applications, College of Chemistry and Molecular Engineering, Peking University, Beijing 100871, People's Republic of China

ABSTRACT Controllable synthesis of macroscopically uniform, high-quality monolayer MoS_2 is crucial for harnessing its great potential in optoelectronics, electrocatalysis, and energy storage. To date, triangular MoS_2 single crystals or their polycrystalline aggregates have been synthesized on insulating substrates of SiO_2/Si, mica, sapphire, *etc.*, *via* portable chemical vapor deposition methods. Herein, we report a controllable synthesis of dendritic, strictly monolayer MoS_2 flakes possessing tunable degrees of fractal shape on a specific insulator, $SrTiO_3$. Interestingly, the dendritic monolayer MoS_2, characterized by abundant edges, can be transferred intact onto Au foil electrodes and serve as ideal electrocatalysts for hydrogen evolution reaction, reflected by a rather low Tafel slope of ~73 mV/decade among CVD-grown two-dimensional MoS_2 flakes. In addition, we reveal that centimeter-scale uniform, strictly monolayer MoS_2 films consisting of relatively compact domains can also be obtained, offering insights into promising applications such as flexible energy conversion/harvesting and optoelectronics.

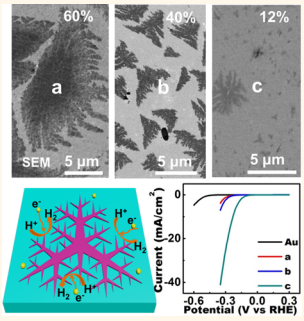

KEYWORDS: molybdenum disulfide · monolayer · $SrTiO_3$ · hydrogen evolution reaction · dendritic crystal growth

As a primary member of the transition metal dichalcogenide family,[1−3] semiconducting monolayer molybdenum disulfide (MoS_2) exhibits a plethora of intriguing properties, such as indirect-to-direct band-gap tunability from bulk to monolayer,[4] coupled spin and valley physics,[5] tunable band structure with strain,[6] and highly reactive edge sites for hydrogen evolution reaction (HER).[7−9] All these properties, complementary or even superior to that of semimetallic graphene,[10] have prompted unlimited applications of monolayer MoS_2 in electronics,[11] optoelectronics,[12] electrocatalysis,[13−19] *etc.*

For engineering such applications, controllable synthesis of macroscopically uniform monolayer MoS_2 layers is the most essential issue. Initial studies employing top-down methods of micromechanical exfoliation[20] and ionic intercalation[21] nevertheless resulted in uncontrollable film thickness and domain size. Recently, several bottom-up approaches, such as decomposition of thiomolybdates,[22] sulfurization of transition metals[23] or metal oxide film,[24] and physical vapor deposition,[25] have been developed, aiming at the surface-bound growth of MoS_2 on insulating substrates, still disallowing controllable synthesis with desired thickness uniformity, crystal quality, and domain size.

Compared with the techniques mentioned above, chemical vapor deposition (CVD) has been proven to be a more suitable method for synthesizing monolayer or few-layer MoS_2[26−35] due to its broad tunability of the growth parameters. Single-crystalline MoS_2 triangles or their polycrystalline aggregates have been realized on various insulating substrates, such as silicon dioxide, mica, and sapphire. Recently, CVD-based few-layer flakes and vertically aligned layers have also been reported on conductive glassy carbon or carbon fiber electrodes,

* Address correspondence to yanfengzhang@pku.edu.cn.

Received for review June 24, 2014 and accepted July 17, 2014.

Published online July 17, 2014
10.1021/nn503412w

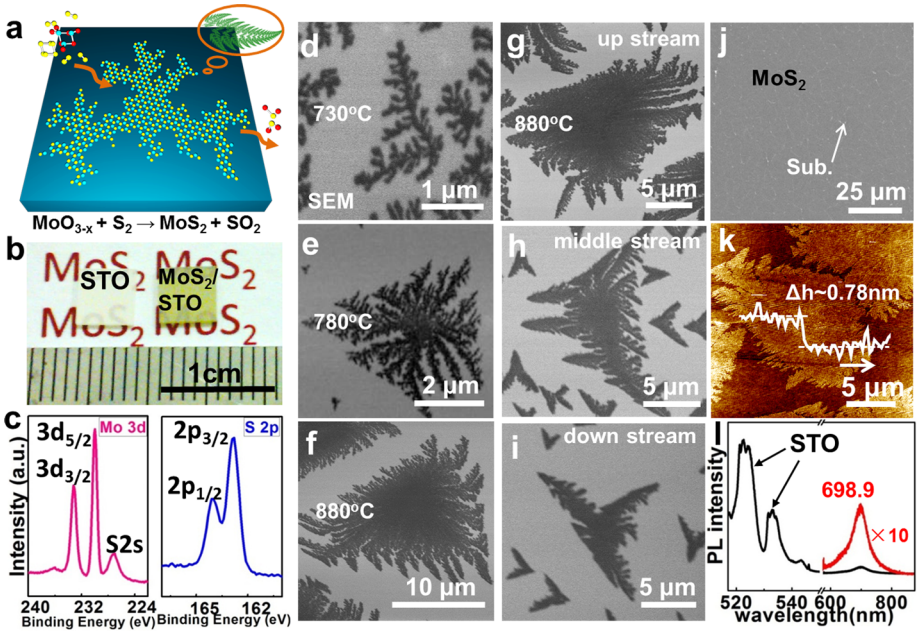

Figure 1. LPCVD synthesis of MoS_2 on STO. (a) Schematic view of the surface growth. (b) Photograph of STO before and after MoS_2 growth. (c) X-ray photoemission spectroscopy (XPS) data of MoS_2 on STO. (d–f) SEM images showing the disparate shapes of MoS_2 flakes synthesized under various growth temperature of 730, 830, and 880 °C, respectively. (g–i) SEM morphologies of three MoS_2 samples synthesized at the same growth procedure (at 880 °C) but with different source–substrate distances (D_{ss}) of 10.0, 10.5, and 11.0 cm, respectively. (j) SEM morphology of a nearly complete monolayer MoS_2 film. (k) AFM image and corresponding section view along the arrow showing a monolayer flake (~0.78 nm in apparent height). (l) PL spectra of as-grown MoS_2 sample and a 10 times magnified A excitonic peak as an inset.

extending the application of CVD-grown MoS_2 for HER.[7,36–38] The number of edge sites,[7] the microscopic structure,[37] the film thickness,[38] and the interface interaction between MoS_2 and substrates[39,40] were considered to be the influential factors for HER efficiency. In this case, the batch production of strictly monolayer, nanosized MoS_2 flakes or films with abundant edge sites, as well as the selection of an appropriate substrate, should be essential for advanced HER efficiency and hence for its practical applications.

Herein, using a low-pressure chemical vapor deposition (LPCVD) method, we report, for the first time, the controllable growth of dendritic MoS_2 on a single crystal substrate of $SrTiO_3$ (STO(100)). The as-grown MoS_2 flakes or films possess the unique trait of strictly one atomic layer, coverage tunable from submonolayer to complete monolayer, and flake shape variable from fractal to nearly compact, by adjusting the growth parameters. We further demonstrate that the MoS_2 on STO(100) can be transferred intact onto other arbitrary substrates such as SiO_2/Si, quartz, PET, and even polycrystalline Au foil substrates. Notably, this transfer process opens up the possibility to engineer the applications of CVD monolayer MoS_2 in the two distinct sectors of electrocatalysis and flexible optoelectronics. As expected, a rather high HER efficiency has been achieved for the fractal-shaped, nanosized MoS_2 flakes transferred on Au foil electrodes even at a relatively low coverage.

RESULTS AND DISCUSSION

The MoS_2 monolayers were synthesized on STO(100) using a homemade (LPCVD) system.[41] The schematic view in Figure 1a depicts the related chemical reaction: MoO_3 was partially reduced by sulfur vapor to form volatile suboxide species MoO_{3-x}, which was further sulfurized to give rise to the formation of MoS_2 on STO (for more details see Supporting Information Figure S1). The macroscopical photograph in Figure 1b clearly presents color contrasts (white and ochre) of samples before and after growth, which may indicate the formation of MoS_2. This was further confirmed by X-ray photoelectron spectroscopy (XPS) data (Figure 1c), with the occurrence of Mo $3d_{5/2}$ and $3d_{3/2}$ states at binding energies of 230.0 and 233.2 eV and $2p_{3/2}$ and $2p_{1/2}$ states of S at 162.8 and 164.1 eV, respectively, typical for MoS_2 films.[24]

Under different growth temperatures of 730, 830, and 880 °C (Figures 1d–f), it is also fascinating to see that the shape of the MoS_2 flakes can vary from highly fractal to relatively compact ones, as featured by scanning electron microscope (SEM) images (also see Figure S2). The morphology evolution reveals that higher growth temperatures could be beneficial to the surface migration of precursors and the crystallization of MoS_2 flakes. Moreover, the source–substrate distance (D_{ss}) contributes another important factor that affects the flake morphology (Figures 1g–i). With increasing D_{ss} from 10.0 cm to 10.5 cm to 11.0 cm, the domain sizes for the MoS_2 flakes are clearly decreased, while the fractal

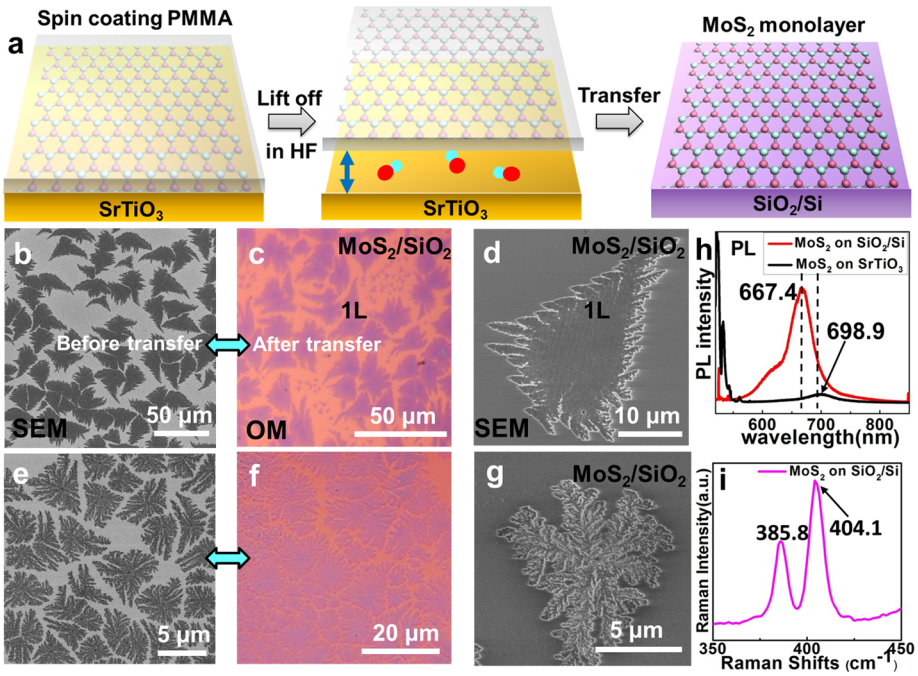

Figure 2. Perfect transference of as-grown quasi-dendritic MoS_2 flakes onto SiO_2/Si. (a) Schematic illustration of the transfer process. (b) SEM image of as-grown monolayer MoS_2 flakes. (c, d) Optical and SEM images of several and a single MoS_2 flake on SiO_2/Si, respectively. (e) SEM image of as-grown dendritic monolayer MoS_2 flakes. (f, g) Optical and SEM images of several and a single dendritic MoS_2 flake on SiO_2/Si, respectively. (h) PL spectra of monolayer MoS_2 flakes before and after transference. (i) Typical Raman spectra of transferred monolayer MoS_2 flakes. The samples were synthesized at the growth temperature of 880 and 780 °C for b and e, respectively.

degree is much enhanced. In addition, a similar growth feature was also obtained for MoS_2 synthesized on STO(111) (shown in Figure S3).

As aforementioned, MoS_2 grown on STO usually presents rather fractal shapes with tortuous edges even under an elevated growth temperature of 880 °C, which is probably mediated by a relatively strong interface interaction and a diffusion-limited-aggregation process[42] (comparison of MoS_2 growth simultaneously on STO and sapphire is provided in Figure S4). Otherwise, it is worth mentioning that full monolayer MoS_2 can be obtained under a growth temperature of 880 °C with a shorter D_{ss} of 9.0 cm (Figure 1j).

Atomic force microscopy (AFM) was employed to evaluate the detailed edge morphology and the thickness of MoS_2 layers on STO (Figure 1k). It is intriguing to see that the edge of the MoS_2 flake seems highly rough even at an elevated growth temperature of 880 °C. An apparent height of ~0.78 nm is observed from the AFM section-view analysis across the film edge, indicative of its monolayer nature[26,43] (more supporting AFM images of dendritic MoS_2 flakes are in Figure S5). Moreover, in the photoluminescence (PL) data (Figure 1l), the A excitonic emission occurs at ~698.9 nm, providing direct proof of the formation of a MoS_2 layer, and E^1_{2g} and A_{1g} phonon modes of MoS_2 are concealed by the STO signal (also see Figure S6).

Transfer of MoS_2 layers to other arbitrary substrates such as SiO_2/Si is thus highly demanded for unraveling their intrinsic spectroscopic properties, as well as for fulfilling their disparate application potentials. The utilized transfer process is schematically illustrated in Figure 2a and discussed in the Methods section.[44,45] Surprisingly, the shapes of the quasi-dendritic flakes seem nearly unchanged prior to (Figure 2b) and after the transfer (Figures 2c,d) process, as suggested by a perfect preservation of the rough edges. Similarly, Figure 2e−g exhibit intact morphologies of the dendritic MoS_2 flakes before and after the transfer. Moreover, a series of aligned wrinkle-like contrasts appear on the transferred MoS_2 (Figure 2d), which might be due to the duplication of the substrate steps and was maintained after transfer. In this regard, nearly intact transfer of monolayer MoS_2 can be realized with the current method (more details in Figure S7).

PL and Raman measurements were then performed on the transferred films on SiO_2/Si. A more intrinsic A excitonic emission peak appears with an intensity almost 10 times higher than that of as-grown MoS_2 on STO, with the peak position blue-shifted from ~698.9 nm to ~667.4 nm (Figure 2h). The spectra of the transferred sample on SiO_2 is in good agreement with that of monolayer MoS_2 synthesized on SiO_2.[26] The blue-shift of the A excitonic peak before and after the transfer process is probably attributed to either the released interface strain effect or the decreased interface charging effect. In addition, two Raman peaks (Figure 2i), corresponding to E^1_{2g} and A_{1g} phonon modes, occur for the transferred MoS_2 at ~385.8

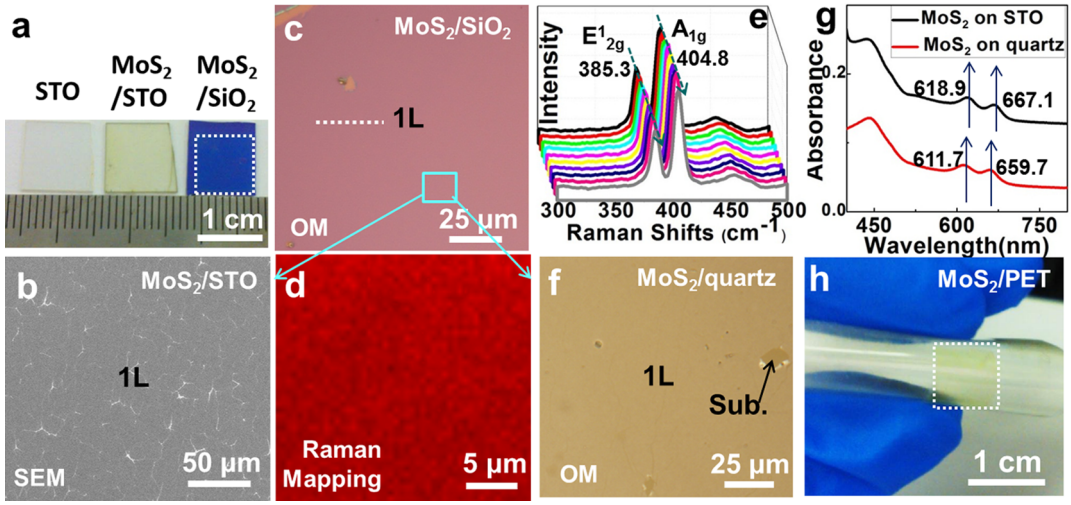

Figure 3. Characterization of centimeter-scale uniform monolayer MoS_2 films on STO and after transference onto SiO_2/Si, quartz, and PET substrates. (a) Photograph of bare STO and nearly complete monolayer MoS_2 on STO and on SiO_2/Si after transfer. (b) SEM image of nearly monolayer as-grown MoS_2. (c, d) Optical photograph of the sample after transference onto SiO_2/Si and Raman mapping of the box region in c with A_{1g} peak integration from 400 to 430 cm^{-1} by a 514 nm laser. (e) Single-point Raman spectra extracted randomly from d. (f) Optical photograph of monolayer MoS_2 transferred on quartz. (g) UV−vis spectra of monolayer MoS_2 on quartz (upper red curve) and on STO (lower black curve). (h) Photograph of monolayer MoS_2 transferred on flexible PET substrates. The growth temperature of the utilized sample was set at ~880 °C with an appropriate D_{ss}.

and ~404.1 cm^{-1}, respectively, with their difference (~18.3 cm^{-1}) corresponding well with that of monolayer MoS_2.[43,46] These spectroscopy data establish the monolayer nature of the synthesized MoS_2 films on STO(100), as well as the alleviated interface interaction for transferred MoS_2/SiO_2 with regard to that of as-grown MoS_2/STO (see Figure 1l).

It is fascinating to find that, through a prolonged growth time, the relatively compact monolayer MoS_2 flakes can patch with each other to form a nearly complete layer on STO (photograph in Figure 3a) at an elevated temperature. This can be verified by the close-up SEM view in Figure 3b, showing a nearly uniform contrast. Moreover, the corresponding optical microscopy (OM) image (Figure 3c) after sample transfer onto SiO_2/Si explicitly shows a uniform pink color (distinct from the rarely observed void down to the substrate showing a khaki color), once again suggestive of its uniform coverage (more supporting SEM images are in Figure S8). Further Raman mapping and single-point data present nearly uniform color contrasts of the A_{1g} peak intensity and nearly fixed locations of the two characteristic peaks (E^1_{2g}, A_{1g}) at 385.29 ± 0.09 and 404.81 ± 0.06 cm^{-1} (Figure 3d,e) and fixed fwhm's for the two peaks of 11.11 ± 0.28 and 10.07 ± 0.14 cm^{-1}, respectively, providing more straightforward evidence of the high thickness uniformity, as well as the monolayer nature of the MoS_2 grown on STO(100).

In addition, the obtained monolayer MoS_2 films were also transferred intact onto quartz substrates, as characterized by the rather uniform OM contrast (Figure 3f) (more information in Figure S9). Then, the UV−vis absorption feature of as-grown and transferred samples can be collected and compared (Figure 3g). The spectrum for MoS_2 as-grown on STO (black curve in Figure 3g) exhibits two excitonic absorption bands, at 667.1 nm (1.86 eV) and 618.9 nm (2.00 eV), respectively, with the energy difference in good agreement with the theoretical value for monolayer MoS_2 (0.148 eV).[47] In contrast, the spectrum for transferred MoS_2 on quartz substrates shows two excitonic absorption bands at 659.7 and 611.7 nm, both blue-shifted by ~20 meV (red curve in Figure 3g), which probably indicate a reduced interface interaction after the sample transfer and a macroscopic uniformity of the monolayer film. More interestingly, this atomic layer thin semiconducting film can also be transferrable onto flexible PET substrates, therefore showing application potentials in the fields of flexible energy conversion/harvesting and optoelectronic and electrocatalytic devices (Figure 3h).

In a further step, it is critical to know the crystallinity of the rough-edged monolayer MoS_2 flakes. To this end, the MoS_2 flakes were then transferred onto a carbon film supported by copper grids for transmission electron microscopy (TEM) investigations. The bright-field image in Figure 4a presents three individual flakes with rather crooked edges. The corresponding dark-field image reveals only two types of domain orientations, as coded by magenta and cyan colors (Figure 4b), which were deduced by selective area electron diffraction (SAED) patterns collected both from inside a flake (area 1 of 5 × 5 μm^2), giving only one set of diffraction spots (Figure 4c), and from two neighboring flakes (in area 2, Figure 4d), presenting two lattices rotated by ~30° to each other. Note that the corresponding SAED

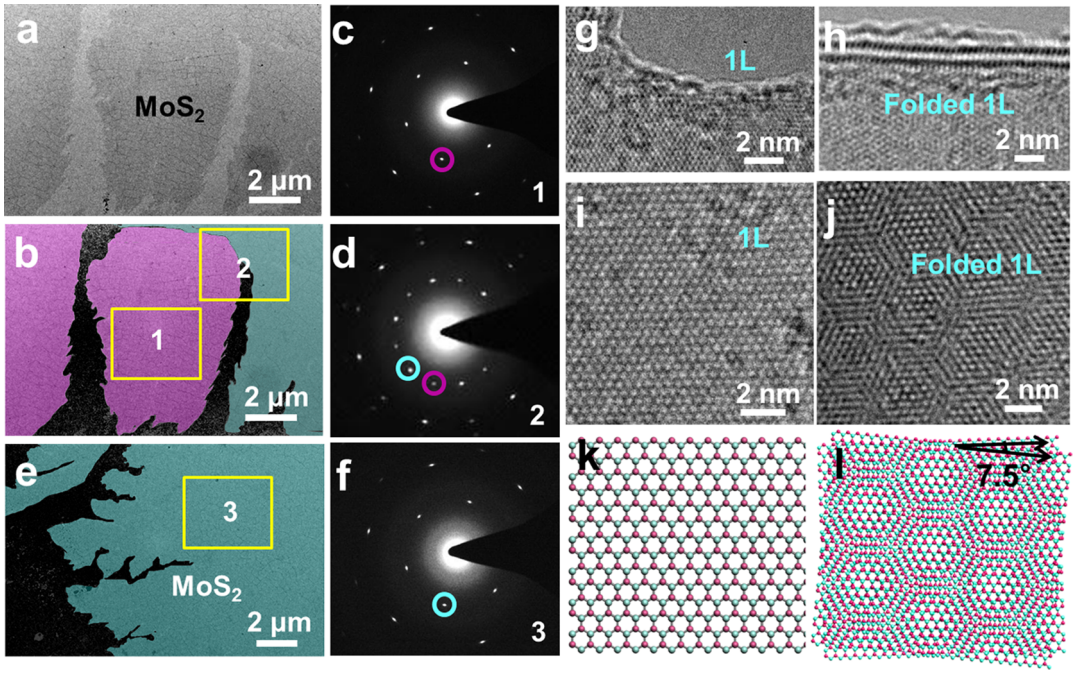

Figure 4. High-resolution transmission electron microscopy (HRTEM) characterizations of the MoS_2 flakes. (a) Bright-field TEM image of monolayer MoS_2 flakes. (b, e) False color dark-field TEM images of monolayer MoS_2 flakes. (c, d, f) Selected area electron diffraction (SAED) patterns recorded from b and e labeled with 1, 2, and 3, respectively. (g, h) HRTEM images around a void and around a folded edge, respectively. (i, k) HRTEM image and atomic model of monolayer MoS_2. (j, l) HRTEM image and atomic model of the moiré pattern. The used samples were synthesized at the growth temperature of ~880 °C.

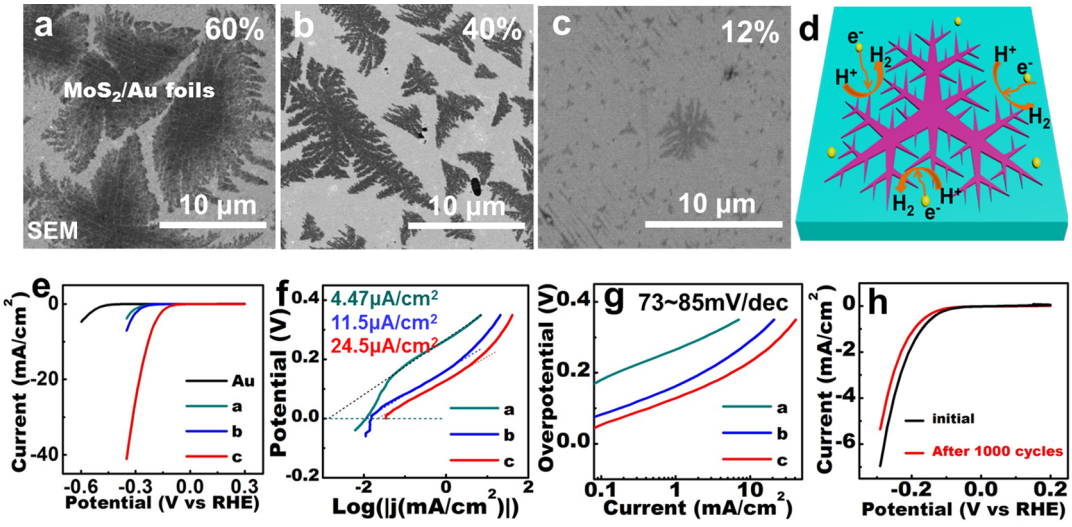

Figure 5. HER activity of dendritic monolayer MoS_2 flakes transferred onto Au foils. (a–c) SEM images of monolayer MoS_2 flakes on Au foils with coverages of 60%, 40%, and 12% and domain sizes of ~10 μm, ~5 μm, and ~800 nm (in envelope edge length), respectively. (d) Schematic view illustrating the edges of fractal monolayer MoS_2 flakes as active catalytic sites for HER. (e) Polarization curves of bare Au foil and MoS_2/Au foils (for samples a–c). (f) Calculated exchange current densities by applying an extrapolation method to Tafel plots. (g) Corresponding Tafel plots. (h) Durability test for the catalysts. The growth temperatures of samples a, b, and c were set at ~ 880, ~780, and ~750 °C, respectively.

pattern of a nearly dendritic flake edge (Figure 4e,f) is also obtained to reveal only one set of diffraction spots, strongly indicative of its quasi-single-crystal nature (or at least consistent orientation).

High-resolution transmission electron microscopy (HRTEM) measurements were then carried out to characterize the monolayer thickness and the crystal quality of the MoS_2 samples. The images captured from the edge of a broken hole (Figure 4g,i), showing a line shape contrast at the film edge and perfect triangular lattices nearby, address its monolayer nature and its perfect crystal quality. In contrast, TEM results achieved at a folded edge (Figure 4h–j) present moiré patterns due to a relative rotation of ~7.5°,

as illustrated by the models shown in Figure 4k,l (also see Figure S10).

The derived fractal monolayer MoS_2 flakes decorated with abundant edges were then considered to serve as electrocatalysts for HER. It is well known that electrocatalytic activity for hydrogen evolution reaction was reported to correlate linearly with the number of edge sites on the MoS_2 catalysts.[7] Fractal MoS_2 flakes with dendritic branches probably provide many more active edge sites than regular triangle flakes with similar flake sizes. Thereby, such dendritic flakes should be suitable for applications in HER. A typical electrode of Au foils was selected, and the intact transfer of various samples onto the electrodes was evidenced by SEM observations (Figure 5a–c). Herein, three samples with sequentially decreased domain sizes of ~10 μm, ~5 μm, and ~800 nm, yet improved edge roughness or edge length, were displayed and used for HER measurements. This is because, according to previous theoretical[8] and experimental results,[9] the HER activity relates closely to the reactive edge density of the MoS_2 flake (with sulfide Mo edges), while the basal surface is catalytically inert (schematic in Figure 5d).

The polarization curves for these MoS_2 samples are shown in Figure 5e. A minimum HER efficiency occurs for sample a (line a in Figure 5e) reflected by an onset potential (η) of −0.278 V, with regard to samples b, c (line b and c in Figure 5e) with sequentially improved values of −0.247 and −0.100 V, respectively. Meanwhile, the exchange current densities of the samples were revealed to be ~4.47, 11.5, and 24.5 $\mu A/cm^2$, respectively (Figure 5f). Note that, sample c exhibits a rather high exchange current density even at a rather low coverage of ~12%, suggestive of the high reactivity of the fractal monolayer MoS_2 flakes in HER.

Moreover, the corresponding Tafel plots were also extracted to evaluate the efficiency of the catalysts (Figure 5g), which show disparate values of ~85, 79, and 73 mV/decade, respectively. The value of ~73 mV/decade again occurs for sample c, which is also much lower than that of the reported value for few-layer CVD MoS_2 grown on glassy carbon electrodes (140–145 mV/decade).[38] The rather high HER efficiency may be explained from the extra high active density related to the dendritic edges, as well as a perfect conductance between MoS_2 and Au electrodes. Note that 1T-phase MoS_2 nanosheets are regarded as more efficient electrocatalysts than their counterpart 2H-phase nanosheets (such as CVD samples), since the active sites of 1T-MoS_2 are not limited to the edges (the case for 2H-MoS_2), but cover the whole basal planes. The HER performance of the dendritic 2H-MoS_2 on Au electrodes is comparable with that of chemically exfoliated 2H-MoS_2 on glassy carbon electrodes (Tafel slope of 75–85 mV/dec).[19]

The reproducible polarization plot even after 1000 voltammetry (CV) cycles was also acquired to further address the perfect durability of the electrocatalysts (Figure 5h). Moreover, the electrical impedance of the samples was obtained by Nyquist plots in Figure S11. In brief, the MoS_2 flakes prepared in this study possess the unique features of centimeter-scale uniform, strictly monolayer, transferable to other arbitrary substrates, high crystal quality, low cost, and, most importantly, high density active sites, making it a perfect substitute for Pt in HER.

CONCLUSION

In summary, we have achieved the LPCVD synthesis of MoS_2 on a brand new substrate, STO. First, the obtained dendritic, transferable, monolayer MoS_2 flakes present rather high edge activity sites, in remarkable contrast with the traditional sharp-edged triangular flakes, making it a perfect candidate for highly efficient electrocatalysis in HER. Second, the monolayer MoS_2 film is transferrable onto arbitrary substrates such as SiO_2/Si, quartz, and PET, which opens up wider application potentials in optoelectronics, solar cells, electrocatalysis, *etc*. Finally, the directly grown single-layer MoS_2 on STO is expected to present some unforeseen properties such as superconductivity, considering the unique trait of STO itself and its interface with only atomic layer thin MoS_2.

METHODS

MoS_2 Growth and Transfer. The growth was performed inside a multi-temperature-zone tube furnace (Lindberg/Blue M) equipped with a 1-in.-diameter quartz tube. Sulfur powder was placed outside the hot zone and mildly sublimated at ~100 °C. MoO_3 powder (Alfa Aesar, purity 99.9%) and STO substrates ((100) and (111) oriented single crystals) were successively placed inside the hot center. Argon gas (50 standard cubic centimeter per minute (sccm)) was used to convey MoO_{3-x} vapor species to the downstream substrates. The growth pressure was set at 30 Pa, and growth time is ~60 min, with growth temperature of MoO_3 and the substrate of ~530 and ~880 °C, respectively. The as-grown MoS_2 samples were transferred onto arbitrary substrates with a commonly used method. First, poly(methyl methacrylate) (PMMA) was spin coated on MoS_2/STO as support, and then the backside STO was etched by a concentrated HF solution. Last, a fresh SiO_2/Si substrate or other substrates were then used to "fish out" the PMMA-capped MoS_2 film, followed by drying it on a hot-plate (100 °C for 10 min) and removing the PMMA by acetone.

Characterization of Monolayer MoS_2. Optical microscopy (Olympus DX51), Raman spectroscopy (Horiba, LabRAM HR-800), AFM (Vecco Nanoscope IIIa), SEM (Hitachi S-4800; acceleration voltage, 5–30 kV), and TEM (JEOL JEM-2100F LaB6; acceleration voltage, 200 kV) were used to characterize the sample. A carbon film supported on copper grids was used for TEM characterization.

Electrochemical Measurements. All of the electrochemical measurements were performed in a three-electrode system on an electrochemical workstation (CHI660D), using transferred MoS_2

flakes on Au foils as the working electrode, a Pt foil as a counter electrode, and a saturated calomel reference electrode. All of the potentials were calibrated to a reversible hydrogen electrode (RHE). Linear sweep voltammetry with a scan rate of 5 mV/s, from +0.30 to −0.35 V *vs* RHE was conducted in 0.5 M H_2SO_4 (sparged with pure N_2, purity 99.999%). The Nyquist plots were obtained with frequencies ranging from 100 kHz to 0.1 Hz at an overpotential of 10 mV. The impedance data were fitted to a simplified Randles circuit to extract the series and charge-transfer resistances.

Conflict of Interest: The authors declare no competing financial interest.

Acknowledgment. This work was financially supported by National Natural Science Foundation of China (Grant Nos. 51222201, 51290272, 21073003, 21201012, 51121091, 51072004, 51201069) and the Ministry of Science and Technology of China (Grant Nos. 2011CB921903, 2012CB921404, 2012CB933404, 2013CB932603, 2011CB933003), the Keygrant Project of Chinese Ministry of Education (Grant No. 313026), and the Program for New Century Excellent Talents in University (Grant No. NCET-10-0437).

Supporting Information Available: Schematic view of the utilized LPCVD system, supplementary SEM images of MoS_2 prepared on STO(100) and STO(111), crystal structures of STO (100) and STO (111), SEM morphologies of MoS_2 grown on STO and sapphire under the same growth batch, supplementary AFM characterization of dendritic MoS_2 flakes, Raman and PL properties of STO substrates, SEM images of MoS_2 flakes and nearly complete monolayer MoS_2 after transference, supplementary OM images of monolayer MoS_2 transferred on quartz, TEM data of MoS_2, and Nyquist plots of MoS_2 samples. This material is available free of charge *via* the Internet at http://pubs.acs.org.

REFERENCES AND NOTES

1. Wang, Q. H.; Kalantar-Zadeh, K.; Kis, A.; Coleman, J. N.; Strano, M. S. Electronics and Optoelectronics of Two-Dimensional Transition Metal Dichalcogenides. *Nat. Nanotechnol.* **2012**, *7*, 699–712.
2. Chhowalla, M.; Shin, H. S.; Eda, G.; Li, L.-J.; Loh, K. P.; Zhang, H. The Chemistry of Two-Dimensional Layered Transition Metal Dichalcogenide Nanosheets. *Nat. Chem.* **2013**, *5*, 263–275.
3. Huang, X.; Zeng, Z.; Zhang, H. Metal Dichalcogenide Nanosheets: Preparation, Properties and Applications. *Chem. Soc. Rev.* **2013**, *42*, 1934–1946.
4. Mo, S.-K.; Hussain, Z.; Bansil, A.; Shen, Z.-X. Direct Observation of the Transition from Indirect to Direct Bandgap in Atomically Thin Epitaxial $MoSe_2$. *Nat. Nanotechnol.* **2014**, *9*, 111–115.
5. Zeng, H.; Liu, G.-B.; Dai, J.; Yan, Y.; Zhu, B.; He, R.; Xie, L.; Xu, S.; Chen, X.; Yao, W. Optical Signature of Symmetry Variations and Spin-Valley Coupling in Atomically Thin Tungsten Dichalcogenides. *Sci. Rep.* **2013**, *3*, 1608.
6. Shi, H.; Pan, H.; Zhang, Y.-W.; Yakobson, B. I. Quasiparticle Band Structures and Optical Properties of Strained Monolayer MoS_2 and WS_2. *Phys. Rev. B* **2013**, *87*, 155304.
7. Jaramillo, T. F.; Jørgensen, K. P.; Bonde, J.; Nielsen, J. H.; Horch, S.; Chorkendorff, I. Identification of Active Edge Sites for Electrochemical H_2 Evolution from MoS_2 Nanocatalysts. *Science* **2007**, *317*, 100–102.
8. Appel, A. M.; DuBois, D. L.; Rakowski DuBois, M. Molybdenum-Sulfur Dimers as Electrocatalysts for the Production of Hydrogen at Low Overpotentials. *J. Am. Chem. Soc.* **2005**, *127*, 12717–12726.
9. Bonde, J.; Moses, P. G.; Jaramillo, T. F.; Nørskov, J. K.; Chorkendorff, I. Hydrogen Evolution on Nano-Particulate Transition Metal Sulfides. *Faraday Discuss.* **2009**, *140*, 219–231.
10. Berger, C.; Song, Z.; Li, X.; Wu, X.; Brown, N.; Naud, C.; Mayou, D.; Li, T.; Hass, J.; Marchenkov, A. N.; *et al*. Electronic Confinement and Coherence in Patterned Epitaxial Graphene. *Science* **2006**, *312*, 1191–1196.
11. Wu, S.; Ross, J. S.; Liu, G.-B.; Aivazian, G.; Jones, A.; Fei, Z.; Zhu, W.; Xiao, D.; Yao, W.; Cobden, D.; *et al*. Electrical Tuning of Valley Magnetic Moment through Symmetry Control in Bilayer MoS_2. *Nat. Phys.* **2013**, *9*, 149–153.
12. Mak, K. F.; He, K.; Shan, J.; Heinz, T. F. Control of Valley Polarization in Monolayer MoS_2 by Optical Helicity. *Nat. Nanotechnol.* **2012**, *7*, 494–498.
13. Kibsgaard, J.; Chen, Z.; Reinecke, B. N.; Jaramillo, T. F. Engineering the Surface Structure of MoS_2 to Preferentially Expose Active Edge Sites for Electrocatalysis. *Nat. Mater.* **2012**, *11*, 963–969.
14. Chang, Y. H.; Lin, C.-T.; Chen, T.-Y.; Hsu, C.-L.; Lee, Y.-H.; Zhang, W.; Wei, K.-H.; Li, L.-J. Highly Efficient Electrocatalytic Hydrogen Production by MoS_x Grown on Graphene-Protected 3D Ni Foams. *Adv. Mater.* **2013**, *25*, 756–760.
15. Huang, X.; Zeng, Z.; Bao, S.; Wang, M.; Qi, X.; Fan, Z.; Zhang, H. Solution-Phase Epitaxial Growth of Noble Metal Nanostructures on Dispersible Single-Layer Molybdenum Disulfide Nanosheets. *Nat. Commun.* **2013**, *4*, 1444.
16. Lukowski, M. A.; Daniel, A. S.; Meng, F.; Forticaux, A.; Li, L.; Jin, S. Enhanced Hydrogen Evolution Catalysis from Chemically Exfoliated Metallic MoS_2 Nanosheets. *J. Am. Chem. Soc.* **2013**, *135*, 10274–10277.
17. Xie, J.; Zhang, H.; Li, S.; Wang, R.; Sun, X.; Zhou, M.; Zhou, J.; Lou, X.; Xie, Y. Defect-Rich MoS_2 Ultrathin Nanosheets with Additional Active Edge Sites for Enhanced Electrocatalytic Hydrogen Evolution. *Adv. Mater.* **2013**, *25*, 5807–5813.
18. Xie, J.; Zhang, J.; Li, S.; Grote, F.; Zhang, X.; Zhang, H.; Wang, R.; Lei, Y.; Pan, B.; Xie, Y. Controllable Disorder Engineering in Oxygen-Incorporated MoS_2 Ultrathin Nanosheets for Efficient Hydrogen Evolution. *J. Am. Chem. Soc.* **2013**, *135*, 17881–17888.
19. Voiry, D.; Salehi, M.; Silva, R.; Fujita, T.; Chen, M.; Asefa, T.; Shenoy, V. B.; Eda, G.; Chhowalla, M. Conducting MoS_2 Nanosheets as Catalysts for Hydrogen Evolution Reaction. *Nano Lett.* **2013**, *13*, 6222–6227.
20. Britnell, L.; Ribeiro, R.; Eckmann, A.; Jalil, R.; Belle, B.; Mishchenko, A.; Kim, Y.; Gorbachev, R.; Georgiou, T.; Morozov, S. Strong Light-Matter Interactions in Heterostructures of Atomically Thin Films. *Science* **2013**, *340*, 1311–1314.
21. Coleman, J. N.; Lotya, M.; O'Neill, A.; Bergin, S. D.; King, P. J.; Khan, U.; Young, K.; Gaucher, A.; De, S.; Smith, R. J.; *et al*. Two-Dimensional Nanosheets Produced by Liquid Exfoliation of Layered Materials. *Science* **2011**, *331*, 568–571.
22. Liu, K.-K.; Zhang, W.; Lee, Y.-H.; Lin, Y.-C.; Chang, M.-T.; Su, C.-Y.; Chang, C.-S.; Li, H.; Shi, Y.; Zhang, H.; *et al*. Growth of Large-Area and Highly Crystalline MoS_2 Thin Layers on Insulating Substrates. *Nano Lett.* **2012**, *12*, 1538–1544.
23. Zhan, Y.; Liu, Z.; Najmaei, S.; Ajayan, P. M.; Lou, J. Large-Area Vapor-Phase Growth and Characterization of MoS_2 Atomic Layers on a SiO_2 Substrate. *Small* **2012**, *8*, 966–971.
24. Wang, X.; Feng, H.; Wu, Y.; Jiao, L. Controlled Synthesis of Highly Crystalline MoS_2 Flakes by Chemical Vapor Deposition. *J. Am. Chem. Soc.* **2013**, *135*, 5304–5307.
25. Feng, Q.; Zhu, Y.; Hong, J.; Zhang, M.; Duan, W.; Mao, N.; Wu, J.; Xu, H.; Dong, F.; Lin, F.; *et al*. Growth of Large-Area 2D $MoS_{2(1-x)}Se_{2x}$ Semiconductor Alloys. *Adv. Mater.* **2014**, *26*, 2648–2653.
26. Lee, Y. H.; Zhang, X. Q.; Zhang, W.; Chang, M. T.; Lin, C. T.; Chang, K. D.; Yu, Y. C.; Wang, J. T. W.; Chang, C. S.; Li, L. J. Synthesis of Large-Area MoS_2 Atomic Layers with Chemical Vapor Deposition. *Adv. Mater.* **2012**, *24*, 2320–2325.
27. van der Zande, A. M.; Huang, P. Y.; Chenet, D. A.; Berkelbach, T. C.; You, Y.; Lee, G.-H.; Heinz, T. F.; Reichman, D. R.; Muller, D. A.; Hone, J. C. Grains and Grain Boundaries in Highly Crystalline Monolayer Molybdenum Disulphide. *Nat. Mater.* **2013**, *12*, 554–561.
28. Najmaei, S.; Liu, Z.; Zhou, W.; Zou, X.; Shi, G.; Lei, S.; Yakobson, B. I.; Idrobo, J.-C.; Ajayan, P. M.; Lou, J. Vapour Phase Growth and Grain Boundary Structure of Molybdenum Disulphide Atomic Layers. *Nat. Mater.* **2013**, *12*, 754–759.
29. Ji, Q.; Zhang, Y.; Gao, T.; Zhang, Y.; Ma, D.; Liu, M.; Chen, Y.; Qiao, X.; Tan, P.; Kan, M.; *et al*. Epitaxial Monolayer MoS_2 on Mica with Novel Photoluminescence. *Nano Lett.* **2013**, *13*, 3870–3877.

30. Lee, Y.-H.; Yu, L.; Wang, H.; Fang, W.; Ling, X.; Shi, Y.; Lin, C.-T.; Huang, J.-K.; Chang, M.-T.; Chang, C.-S. Synthesis and Transfer of Single-Layer Transition Metal Disulfides on Diverse Surfaces. *Nano Lett.* **2013**, *13*, 1852–1857.
31. Jin, W.; Yeh, P.-C.; Zaki, N.; Zhang, D.; Sadowski, J. T.; Al-Mahboob, A.; van der Zande, A. M.; Chanet, D. A.; Dadap, J. I.; Herman, I. P.; *et al*. Direct Measurement of the Thickness-Dependent Electronic Band Structure of MoS_2 Using Angle-Resolved Photoemission Spectroscopy. *Phys. Rev. Lett.* **2013**, *111*, 106801.
32. Liu, H.; Si, M.; Najmaei, S.; Neal, A. T.; Du, Y.; Ajayan, P. M.; Lou, J.; Ye, P. D. Statistical Study of Deep Submicron Dual-Gated Field-Effect Transistors on Monolayer Chemical Vapor Deposition Molybdenum Disulfide Films. *Nano Lett.* **2013**, *13*, 2640–2646.
33. Ling, X.; Lee, Y.-H.; Lin, Y.; Fang, W.; Yu, L.; Dresselhaus, M. S.; Kong, J. Role of the Seeding Promoter in MoS_2 Growth by Chemical Vapor Deposition. *Nano Lett.* **2014**, *14*, 464–472.
34. Gong, Y.; Liu, Z.; Lipni, A. R.; Shi, G.; Lin, J.; Najmaei, S.; Lin, Z.; Elias, A. L.; Berkdemir, A.; You, G.; et al. Band Gap Engineering and Layer-by-Layer Mapping of Selenium-Doped Molybdenum Disulfide. *Nano Lett.* **2014**, *14*, 442–449.
35. Dumcenco, D.; Ovchinnikov, D.; Marinnov, K.; Sanchez, O. L.; Krasnozhon, D.; Chen, M.-W.; Gillet, P.; i. Morral, A. F.; Radenovic, A.; Kis, A. Large-Area Epitaxial Monolayer MoS_2. Preprint at http://arxiv.org/abs/1405.0129, 2014.
36. Kong, D.; Wang, H.; Cha, J. J.; Pasta, M.; Koski, K. J.; Yao, J.; Cui, Y. Synthesis of MoS_2 and $MoSe_2$ Films with Vertically Aligned Layers. *Nano Lett.* **2013**, *13*, 1341–1347.
37. Wang, H.; Lu, Z.; Xu, S.; Kong, D.; Cha, J. J.; Zheng, G.; Hsu, P.-C.; Yan, K.; Bradshaw, D.; Prinz, F. B.; *et al*. Electrochemical Tuning of Vertically Aligned MoS_2 Nanofilms and its Application in Improving Hydrogen Evolution Reaction. *Proc. Natl. Acad. Sci. U.S.A.* **2013**, *110*, 19701–19706.
38. Yu, Y.; Huang, S.-Y.; Li, Y.; Steinmann, S. N.; Yang, W.; Cao, L. Layer-Dependent Electrocatalysis of MoS_2 for Hydrogen Evolution. *Nano Lett.* **2014**, *14*, 553–558.
39. Li, Y.; Wang, H.; Xie, L.; Liang, Y.; Hong, G.; Dai, H. MoS_2 Nanoparticles Grown on Graphene: An Advanced Catalyst for the Hydrogen Evolution Reaction. *J. Am. Chem. Soc.* **2011**, *133*, 7296–7299.
40. Tsai, C.; Abild-Pedersen, F.; Nørskov, J. K. Tuning the MoS_2 Edge-Site Activity for Hydrogen Evolution *via* Support Interactions. *Nano Lett.* **2014**, *14*, 1381–1387.
41. Zhang, Y.; Zhang, Y.; Ji, Q.; Ju, J.; Yuan, H.; Shi, J.; Gao, T.; Ma, D.; Liu, M.; Chen, Y.; *et al*. Controlled Growth of High-Quality Monolayer WS_2 Layers on Sapphire and Imaging Its Grain Boundary. *ACS Nano* **2013**, *7*, 8963–8971.
42. Zhang, Z.; Lagally, M. G. Atomistic Processes in the Early Stages of Thin-Film Growth. *Science* **1997**, *276*, 377–383.
43. Lee, C.; Yan, H.; Brus, L. E.; Heinz, T. F.; Hone, J.; Ryu, S. Anomalous Lattice Vibrations of Single-and Few-Layer MoS_2. *ACS Nano* **2010**, *4*, 2695–2700.
44. Song, J.-G.; Park, J.; Lee, W.; Choi, T.; Jung, H.; Lee, C.; Hwang, S.-H.; Myoung, J.; Jung, J.-H.; Kim, S.-H.; *et al*. Layer-Controlled, Wafer-Scale, and Conformal Synthesis of Tungsten Disulfide Nanosheets Using Atomic Layer Deposition. *ACS Nano* **2013**, *7*, 11333–11340.
45. Sun, J.; Gao, T.; Song, X.; Zhao, Y.; Lin, Y.; Wang, H.; Ma, D.; Chen, Y.; Xiang, W.; Wang, J.; *et al*. Direct Growth of High-Quality Graphene on High-κ Dielectric $SrTiO_3$ Substrates. *J. Am. Chem. Soc.* **2014**, *136*, 6574–6577.
46. Zeng, H.; Dai, J.; Yao, W.; Xiao, D.; Cui, X. Valley Polarization in MoS_2 Monolayers by Optical Pumping. *Nat. Nanotechnol.* **2012**, *7*, 490–493.
47. Zhu, Z.; Cheng, Y.; Schwingenschlögl, U. Giant Spin-Orbit-Induced Spin Splitting in Two-Dimensional Transition-Metal Dichalcogenide Semiconductors. *Phys. Rev. B* **2011**, *84*, 153402.